Received: 22 August 2023 | Revised: 2 January 2024 | Accepted: 2 January 2024

DOI: 10.1002/pc.28130

RESEARCH ARTICLE

Polymer COMPOSITES WILEY

Polymer-based filaments with embedded magnetocaloric Ni-Mn-Ga Heusler alloy particles for additive manufacturing

Álvaro Díaz-García[1] | Jia Yan Law[1] | Łukasz Żrodowski[2] | Bartosz Morończyk[3] | Rafał Wróblewski[3] | Victorino Franco[1]

[1]Departamento de Física de la Materia Condensada, ICMS-CSIC, Universidad de Sevilla, Sevilla, Spain

[2]AMAZEMET, Warsaw, Poland

[3]Faculty of Materials Science and Engineering, Warsaw University of Technology, Warsaw, Poland

Correspondence
Victorino Franco, Departamento de Física de la Materia Condensada, ICMS-CSIC, Universidad de Sevilla, P.O. Box 1065, 41080 Sevilla, Spain.
Email: vfranco@us.es

Funding information
Clean Hydrogen Partnership, Grant/Award Number: 101101461; Air Force Office of Scientific Research, Grant/Award Number: FA8655-21-1-7044; Consejería de Economía, Conocimiento, Empresas y Universidad, Junta de Andalucía, Grant/Award Number: EMC21_00418; Agencia Estatal de Investigación, Grant/Award Number: PID2019-105720RB-I00; POB "Technologie Materiałowe" of Warsaw University of Technology within the Excellence Initiative: Research University (IDUB) Programme

Abstract

One important issue associated to magnetocaloric materials that hinders its technological application is the poor processability and structural integrity of those with the highest performance, usually intermetallics undergoing first-order magnetic phase transitions. Additionally, the performance of these magnetocaloric materials highly depends on the structural stability of the magnetocaloric phase, which is, in many cases, very sensitive to temperature and mechanical processes. Additive manufacturing via the extrusion of polymer-based composites is regarded as a promising way to overcome these issues. A recently presented manufacturing method of encapsulating functional fillers into polymer capsules has been used to produce a composite filament with a large load of magnetocaloric off-stoichiometric Ni_2MnGa Heusler alloy fillers with a uniform distribution throughout the polymer matrix as demonstrated by x-ray tomography characterization. The incorporation of these metallic particles causes changes in the thermal behavior of the polymer as well as an increase in the flowability of the composite with respect to the polymer at the same temperature. The increased flowability of the composites found during manufacturing can be compensated by lowering the extrusion temperatures, making this technique even more convenient for preserving the filler properties, which is an important concern when additive manufacturing magnetocaloric materials. This is confirmed by the magnetic and magnetocaloric behavior of the composites, with responses proportional to the fraction of fillers.

Highlights

- Ultrasonic-atomization produces highly spherical Ni-Mn-Ga Heusler alloy particles.
- Ni-Mn-Ga filled polymer capsules allow a direct extrusion of composites for AM.
- X-ray tomography shows uniform volumetric filler distribution within the filaments.

- Decreased viscosity of the matrix favors the lowering of the processing temperature.
- The low processing temperatures avoid altering the MCE of the alloy fillers.

KEYWORDS
additive manufacturing, composite filaments, magnetocaloric effect

1 | INTRODUCTION

A transition to more environmentally friendly and efficient refrigeration technologies would be very beneficial to reducing pollution and global warming. One of the most promising alternatives is magnetic refrigeration, which has produced prototypes that are 50% more energy efficient than conventional systems, while avoiding the use of the refrigerant gases that contribute to greenhouse and ozone depletion effects.[1–3] However, for magnetic refrigerators to reach the mass market, the competitiveness of current magnetocaloric materials must be increased. The magnetocaloric effect (MCE), on which magnetic refrigerators are based, refers to the temperature change or entropy change exhibited by a magnetic material when magnetized/demagnetized under adiabatic or isothermal conditions, respectively. The strongest manifestation of this effect is observed when a magnetic phase transition occurs as these can have associated significant temperature-dependent changes in magnetization.

Despite high hopes for this field, further research is essential, as there are still no materials that realistically balance performance and cost.[4,5] Currently, materials undergoing first-order phase transitions (FOPT) attract the most attention as these can exhibit a giant MCE performance without depending on critical elements. The family of NiMn-based Heusler alloys is one of the most relevant representatives of this group due to the occurrence of a magnetostructural transformation (typically referred to as martensitic transformation) which consists of a solid-to-solid transition from a martensitic-type structure to an austenitic one upon heating, which has a significant MCE associated to it as well as magnetic shape memory effect.[6–10] In magnetocaloric Heusler alloys, at least one of the phases involved in the martensitic transition is ferromagnetic. Therefore, it is common to also detect in these materials the Curie transition (second-order phase transition) of some of the phases. As in every material undergoing magnetostructural transformation, the thermal hysteresis in magnetocaloric Heusler alloys is a factor that needs to be reduced as it limits their performance when working under cyclic conditions in refrigeration devices.[11–13] Additionally, issues related to poor processability due to the intermetallic nature of these alloys as well as rapid structural degradation caused by repetitive volume changes during the transformation are factors that also limit the applicability of these materials.

As in many other technological areas, additive manufacturing (AM) is becoming a strong alternative to traditional manufacturing methods due to its ability to overcome the issues associated with poor processability and because some of the AM techniques, especially those based on thermoplastic polymers, are broadly accessible nowadays.[14–17] The different AM methods can build parts with virtually no shape constraints, making the manufacturing of intricate microchannel structures that optimize heat exchange in solid state refrigerators feasible, even when made from intrinsically brittle intermetallics.[18,19] AM encompasses techniques that directly print from raw metallic materials,[20,21] but these imply alloy formation during the printing process, which complicates obtaining the appropriate magnetocaloric active phases. Even when starting from pre-alloyed powders, metal AM requires melting the alloy, which in the case of magnetocaloric alloys can cause the alteration or loss of their properties.[22–27] Conversely, the most extended and accessible AM technique, known as fused deposition modeling (FDM), uses a polymer material. This method is gaining more and more attention as these polymeric materials can incorporate multiple types of fillers[28–32] to provide some type of functionality to the built parts (e.g., electrical,[33,34] magnetic,[35–38] optical[39,40]) or an improved mechanical resistance[41,42] while preserving the manufacturing advantages. The low melting temperatures of typical polymers prevent the modification of the properties of the magnetocaloric fillers during fabrication and printing.[43,44] In the present case, the binder polymer in FDM does not contribute to the MCE but it can act as support that maintains the structural consistency of the part as well as protective shell that prevents the corrosion of the magnetocaloric particles. Otherwise, the polymer could be eliminated by performing debinding methods followed by sintering in cases where the presence of polymer is not desired,[45,46] which might require further processes to restore the functional properties of the fillers. In this work, off-stoichiometric Ni_2MnGa Heusler alloy

powder produced by ultrasonic-atomization has been used as functional filler to fabricate polymer-matrix composite filaments for FDM, with filler fractions of 30, 39, and 64 wt%. The recyclability of produced materials is a significant concern nowadays. In this case, it could be even more relevant as we propose the use of metallic particles combined with a thermoplastic polymer. The thermoplastic polymer used in this case is polylactic acid (PLA), which is one of the most used polymers for 3D printing due to its ease of processing and printing. It is considered a biodegradable polymer, which provides numerous options for recycling.[47] In addition, some of the methods commonly used for recycling thermoplastic polymers, such as chemical or thermo-chemical recycling, allow to separate the additives,[48] allowing their reuse. The filament fabrication technique used is based on a recently presented method in which the feedstock for a single-screw extruder is prepared using polymer capsules filled with particles with the desired functionality.[49] This fabrication method eliminates the restrictions of polymer compositions or particle sizes from other techniques, allowing the use of nanoparticles in the cases that would be required. Composite filaments show the same MCE response as that of the raw powder by scaling down due to the mass of the non-contributing polymer. This work shows that composite filaments including high loads of magnetocaloric powder can be manufactured with an excellent uniform distribution of fillers while preserving their functional properties.

2 | MATERIALS AND METHODS

The starting functional magnetocaloric material consisted of off-stoichiometric Ni_2MnGa Heusler alloy powder that was produced through the ultrasonic atomization technique by the Warsaw University of Technology and the company AMAZEMET, both in Poland. This atomization method[50] directly involves the melting of the alloy in the atomizer and is poured onto the surface that vibrates at a specific high frequency, 20 kHz in this case. The vibration of the surface causes the poured molten alloy to separate into fine droplets, which then solidify into spherical particles with sizes that depend on the frequency: the higher the frequency, the smaller the particle size, with all other parameters invariant. The as-atomized powder was further sieved to 100 μm before being used for filament manufacturing.

For the polymeric matrix of the composite filaments, (PLA) was chosen given its ease of processing and printing, both in its pure state and in combination with different types of fillers.[29,44,51,52] The manufacturing of the composite filaments was done according to the encapsulation procedure presented previously in Ref. 49. In summary, capsules of the intended polymer that will conform the composite filaments, PLA in this case, were 3D-printed to be filled with the functional off-stoichiometric Ni_2MnGa fillers. These capsules are semi-oval shaped with sizes of 4–5 mm which matches those of the typical polymer pellets used for filament extrusion. Once filled and sealed, these capsules were directly used in the single-screw extruder 3devo NEXT 1.0 ADVANCED. By changing the dimensions of the capsules, the fraction of polymer in the composite capsules can be controlled, allowing different nominal compositions to be easily obtained. In this case, the filling fraction has been progressively increased from the original 30 wt% of fillers by reducing the wall thickness of the capsules while keeping their total outer volume. The largest filling fraction obtained in this work resulted after reducing the wall thickness of the capsules until they could be 3D printed using just one wall layer of 0.4 mm, which was found not to cause powder leaks. Filaments with a nominal diameter of 2.85 mm were fabricated. As found in previously manufactured PLA filaments containing metallic fillers,[44,49] the temperature of the four heaters of the extruder had to be lowered below the typical values for raw PLA to be able to extrude and spool the composite filaments. This is due to the increased flowability of the composite filaments. For pure PLA, the temperatures of the heaters located along the extrusion path (from the one next to the hopper to the one near the nozzle) are 443, 458, 463, and 453 K (170, 185, 190, and 180°C). For the composite filament with the highest filling fraction, these temperatures had to be reduced to 438, 453, 455, and 445 K (165, 180, 182, and 172°C). This is because filling polymer with some types of spherical particles can cause the viscosity of the composite to drop below that of the pure polymer due to the so-called "ball-bearing" effect since these particles can reduce friction between different polymer layers.[51,53] In this case, lowering the extrusion temperature would be able to restore the viscosity to appropriate values. This may significantly lower energy consumption and cost during mass production. In order to analyze the trend of the composite properties, the content of filler loading was progressively increased from a relatively low fraction of nominally 30 wt% up to a high filling fraction of 65 wt% with an intermediate composition of nominally 40 wt% of fillers.

Morphological and compositional characterization of the sieved powder were conducted by scanning electron microscopy (SEM) using a FEI Teneo microscope that incorporates an energy dispersive x-ray spectroscopy (EDX) detector. The particle distribution of the composite

filament was studied from its cross-section using SEM. An extended microstructural characterization was performed by x-ray tomography experiments with a Zeiss Xradia 610 Versa equipment. The x-ray tomography measurement was performed on a section of the filament (~2 mm length) with the highest filling fraction, using a tube voltage of 100 kV and a 4X objective to provide a pixel size of 3.4 μm. The two components of the composite filaments can be easily distinguished by this technique, given the large atomic number difference between the polymer matrix and the metallic fillers. For a computationally less demanding but still representative image analysis, a cubic volume of 1.5 mm side centered at the filament piece was selected to be processed and analyzed using the free software FIJI with the dedicated suite of plugins MorphoLibJ.[54] The different particles were identified by thresholding and applying the MorphoLibJ algorithm Distance Transform Watershed 3D that allows separating particles in apparent contact that would otherwise be accounted as one. The Analyze 3D Regions tool in MorphoLibJ gives the coordinates of center of mass, surface area and volume of the different identified particles. The volume fraction of fillers was directly determined by dividing the total volume of particles by the volume of the cropped 1.5 mm side cube. For this, cropped particles at the borders of the images were kept. Subsequently, the particles at the borders of the image were eliminated to perform the morphology and interparticle distance analysis. The sphericity of the particles was calculated as:

$$\text{Sphericity} = 36\pi\frac{V^2}{S^3}, \tag{1}$$

where V is the particle volume and S the particle surface area. This formula is normalized to the volume-to-surface ratio of a sphere. In this way, values equal to 1 are obtained for a perfect sphere, while other geometries will have sphericity values lower than 1. Particle sizes were calculated as the diameter of the sphere with the same volume of the particle, that is:

$$d = \left(\frac{6V}{\pi}\right)^{1/3}. \tag{2}$$

The distribution of the distance between particles was obtained using MATLAB to compute the Euclidean distance to the nearest neighbor of each of the points defined by the center of mass of the particles, for which the Delaunay triangulation method was used.[49]

The thermal properties of the raw materials and composites were investigated by thermogravimetric analysis (TGA) with a TA Instruments Q600 thermobalance and by differential scanning calorimetry (DSC) with a TA Instrument Q20 calorimeter. TGA experiments were conducted upon heating at 10 K min^{-1} up to 750 K for both pure PLA and the different composite filaments. At the maximum temperature reached, that is, 750 K, PLA is totally degraded so that the remaining mass in composites is used to get the actual weight fraction of fillers. DSC measurements were performed for raw polymer and powders as well as for composites, with samples sealed into hermetic aluminum pans and measured at a sweeping rate of 10 K min^{-1}.

The magnetic characterization was performed using the vibrating sample magnetometry (VSM) option of a Quantum Design PPMS with applied fields up to 5 T and a Lake Shore 7407 VSM that produces a maximum magnetic field of 1.5 T. The MCE was characterized through the isothermal entropy change, ΔS_{iso}, calculated from isothermal magnetization versus field curves, $M(H)$, by applying the Maxwell relation:

$$\Delta S_{iso} = \mu_0 \int_0^H \left(\frac{\partial M}{\partial T}\right)_{H'} dH', \tag{3}$$

where μ_0 is the permeability of free space and T is the temperature.

Due to the hysteresis that magnetization processes show in the vicinity of FOPTs, a discontinuous protocol was followed to erase the memory of the material prior to the acquisition of each $M(H)$ curve used for calculating ΔS_{iso}.[55–57]

3 | RESULTS AND DISCUSSION

3.1 | Microstructural analysis

Figure 1A presents the SEM image of the powder along with its measured composition of $Ni_{49}Mn_{30.5}Ga_{20.5}$ obtained by EDX. It is noticed that particles are predominantly spherical and that they show a relatively narrow particle size distribution caused by the sieving at a diameter below the original mean particle size. Figure 1B shows the micrograph of the cross-section of the filament with the highest filling (65 wt% nominal fraction). It can be noticed that some particles have come loose from the polymer matrix due to the cutting of the filament for its cross-section characterization. However, it is clearly seen that they are well embedded within the polymer and that the particles are close to each other, which is an indication that a high filling fraction is achieved. Considering the density of the PLA 1.25 and 8.20 g cm^{-3} for the

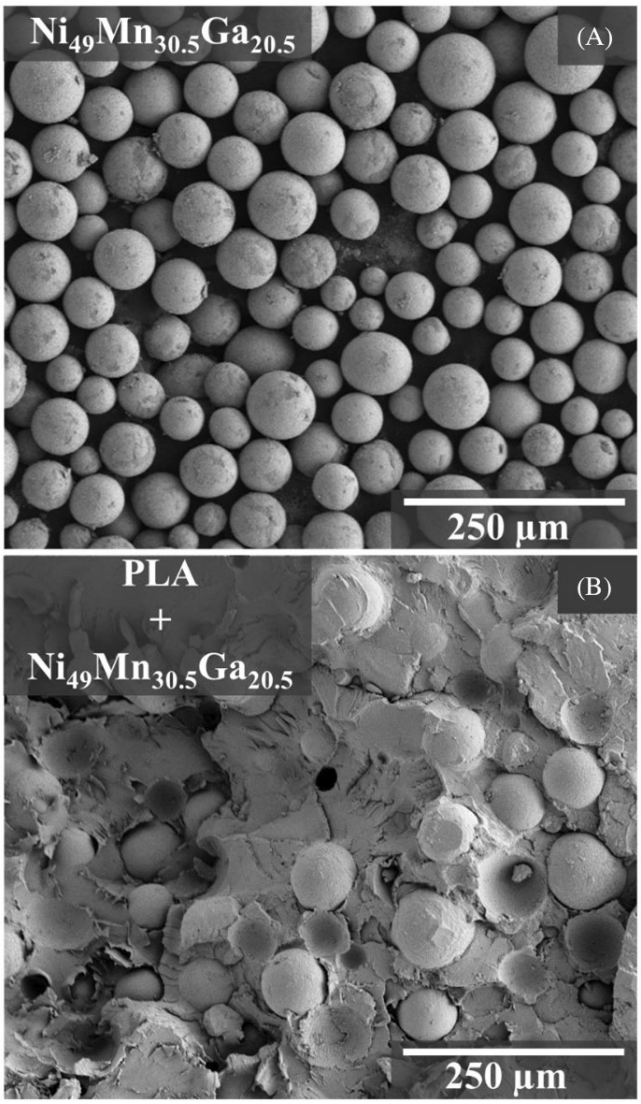

FIGURE 1 (A) Scanning electron micrograph of the ultrasonic-atomized off-stoichiometric Ni_2MnGa Heusler powder showing the composition measured by energy dispersive x-ray spectroscopy. (B) Scanning electron micrograph of the cross section of the composite filament with nominal 65 wt% filling fraction.

Ni-Mn-Ga powder, the nominal volume fraction corresponding to 65 wt% (nominal) of fillers would be ~21 vol%.

The highest-loaded filament in this study (nominal 65 wt%) was further investigated with x-ray tomography for a 3D analysis of its characteristics. The ratio between the total volume of particles within the analyzed cubic volume of 1.5 mm edges reveals a volume fraction of 22.7% for the filament with 65 wt% (nominal) of fillers. This value agrees with the previously estimated 21 vol% of fillers based on the nominal weight concentration and densities of the PLA and fillers.

Figure 2 presents the results of the extended image analysis of the x-ray tomography characterization of the composite. The 3D reconstruction of the particles within the cropped cube of 1.5 mm edges is shown in Figure 2A, where particles at the edges of the cube have been removed. Figure 2A also includes the sphericity distribution, which confirms the good spheroidal shapes of the as-atomized particles as ~65% of them show sphericity values in the 0.9–1 range. The size distribution analysis plotted as a bar graph in panel (B) shows a relatively uniform particle size distribution within 40–80 µm due to sieving with a mesh of 100 µm. More than 96% of the particles have diameters below 100 µm as highlighted from the cumulative frequency plot (presented as the line graph in panel (B)). Particles above that size would be associated to more elongated shapes or particles in contact (due to agglomeration) that image processing could not separate. The computed interparticle distance between the nearest neighbors is shown in panel (C). This distribution fits the amplitude version of the Gaussian distribution, typical of a normally distributed random variable, confirming the even distribution of particles. From the fitting parameters, the expected interparticle distance is 66.7 µm with a variance of 12.2 µm. When comparing panels (B) and (C), it is found that the expected interparticle distance is within the most common particle diameter range of 40–80 µm. This indicates that, despite the even distribution of the particles, close contact between them is expected due to the high filling fraction.

3.2 | Thermal analysis

According to the TGA curves of pure PLA polymer and composite filaments depicted in Figure 3, fractions of fillers of 30, 39, and 64 wt% are obtained for the different composite filaments upon the degradation of the polymer. These results agree with the nominal concentrations. From this point onwards, the composite filaments of this study will be denoted through their experimental filler concentration determined by TGA: 30, 39, and 64 wt%. The maximum temperature used for the extrusion of the 64 wt% filament was 455 K, which is still well below the starting temperature of the degradation of PLA in this composite.

Apart from providing information on the filler concentration in the composite filaments, TGA curves show that the incorporation of these metallic fillers affects the dynamic of PLA thermal degradation by displacing it to lower temperatures. This was previously observed and reported in the literature, in which some of the composite examples are PLA filaments incorporating maraging steel,[51] and $(La,Ce)(Fe,Si,Mn)_{13}$-H fillers.[44] To analyze possible changes in the kinetics of the PLA degradation, the temperature derivatives of the weight fraction curves,

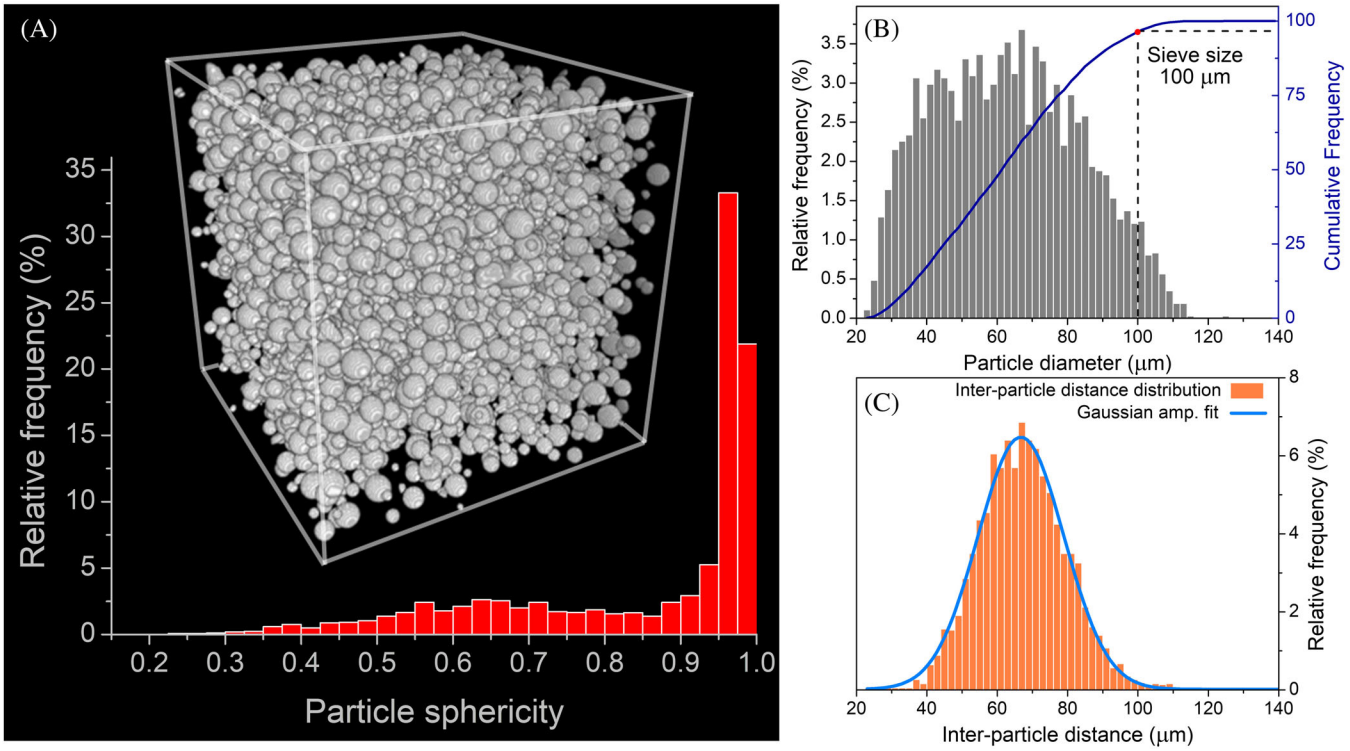

FIGURE 2 (A) 3D reconstruction together with the sphericity distribution from the x-ray tomography characterization of nominal 65 wt% filament, (B) particle diameter distribution, and (C) interparticle distance distribution.

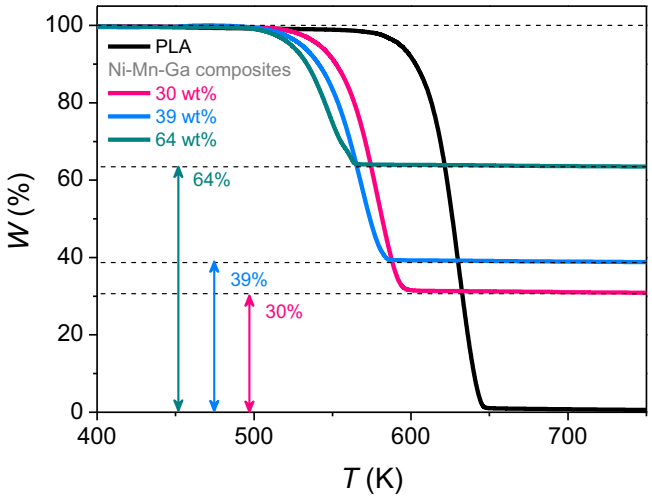

FIGURE 3 Thermogravimetric curves upon heating of pure polylactic acid (PLA) and PLA + Ni-Mn-Ga.

dW/dT, were further calculated and presented in Figure 4A. Replotting them as plots of normalized dW_i/dT versus the temperature difference from their peak temperatures, $T - T_{pk,i}$, presented in Figure 4B simplifies the visualization and comparison. The only noticeable difference among the curves in Figure 4B is in the highest concentration filament, for which a small spike is observed just above the peak temperature. This could be related to a slight slowdown of the degradation in this composite after the maximum, which is suddenly compensated so that the final fall to zero overlaps with the others. This overlap indicates that the kinetics of the degradation remains essentially unchanged for moderate concentrations of fillers.

For the calculated electron per atom ratio, e/a, of 7.65, the Heusler alloy powder is expected to undergo a martensitic transformation near room temperature according to literature.[1,6,7] The DSC results of the raw $Ni_{49}Mn_{30.5}Ga_{20.5}$ powder shown in Figure 5 confirm the presence of the martensitic transition, with heat flow peaks upon cooling and heating that are separated ~20 K that accounts for the thermal hysteresis inherent to this FOPT and with latent heat values of 1.215 and 1.320 J g^{-1}, respectively. At higher temperatures, the characteristic feature of a Curie transition is observed, which corresponds to a change in the heat flow levels instead of a peak with associated latent heat, due to the second-order character of this transition.

Figure 6 shows the DSC curves of pure PLA and composites upon heating. Starting with the DSC curve of pure PLA, the first endothermic peak is related to the glass transition of the polymer, indicating that the PLA undergoes a relaxation process in which it reaches a more thermodynamically stable state. The presence of this transition is due to a rapid cooling down that solidifies

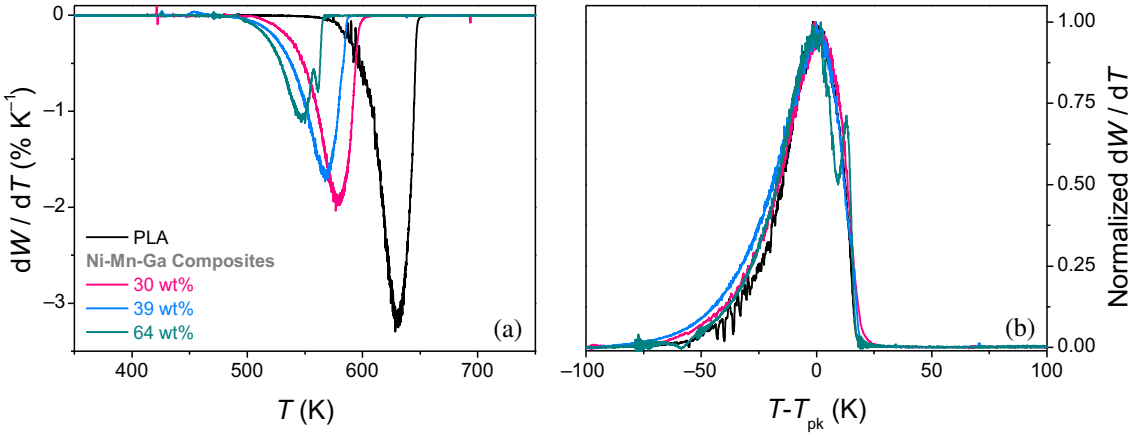

FIGURE 4 (A) Derivative with respect to temperature of the thermogravimetric analysis curves of polylactic acid (PLA) and PLA + Ni-Mn-Ga. (B) Normalized dW/dT curves plotted with respect to a rescaled axis $T - T_{pk}^{TGA}$.

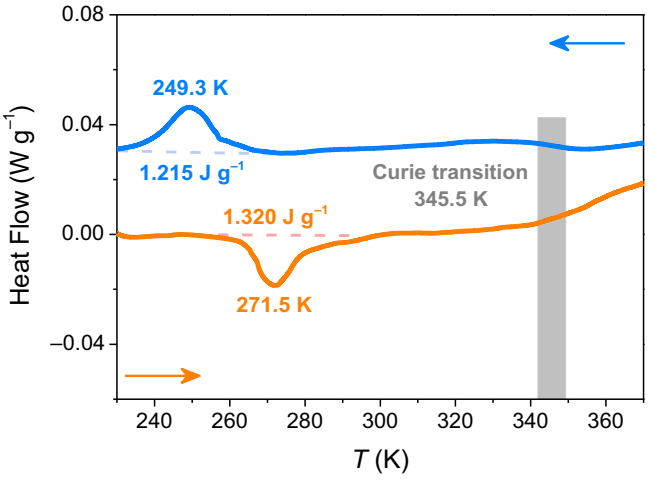

FIGURE 5 Differential scanning calorimetry curves upon cooling and heating of the Ni-Mn-Ga powder.

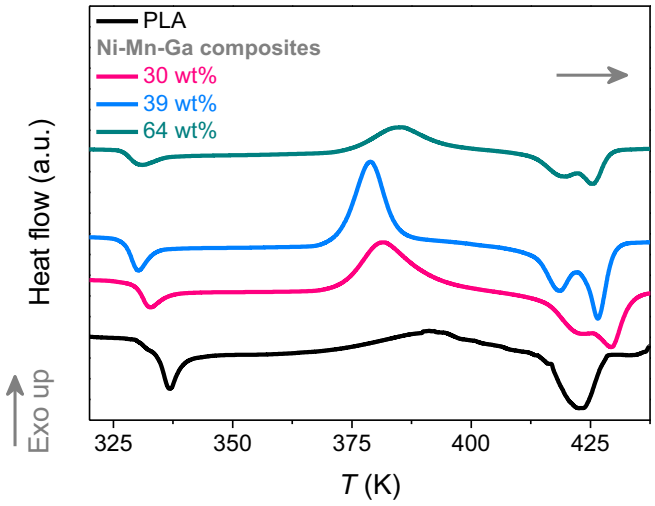

FIGURE 6 Differential scanning calorimetry curves upon heating of as-extruded polylactic acid (PLA) and PLA + Ni-Mn-Ga-composite samples.

the polymer after its melting, typical of the extrusion process. The following exothermic peak is related to the cold crystallization of PLA, which is then followed by melting that is associated with the final endothermic peak. For the PLA + Ni-Mn-Ga composites, analogous DSC peaks are observed though they show some quantitative and qualitative difference. The glass transition of composites, also accompanied by an endothermic peak, shifts to lower temperatures with increasing filling fraction. For composites with 30 and 39 wt% of fillers, the cold crystallization peak becomes sharper and displaces to lower temperatures when compared with pure PLA. It is known that some types of fillers can promote the crystallization of the polymer matrix, advancing it to lower temperatures and making the exothermic process more prominent.[58–60] In this case of PLA, the promoted cold crystallization has an increased fraction of the disordered α' phase associated to it, which has a slightly lower melting temperature, causing the subsequent melting process to divide into two distinguishable peaks.[51,58,61] The curve of the 64 wt% composite is a bit out of the trend, with a cold crystallization peak that gets less relevant, although the presence of the disordered α' is confirmed with the double melting peak. The reason for this decrease of the cold crystallization peak can be explained considering that the total mass of the composite samples is responsible for the heat flow curves; therefore, the processes that take place in the PLA are less visible for the 64 wt% composite because fraction of Ni-Mn-Ga fillers is the largest. Table 1 compiles the values of the relevant temperatures, enthalpy of transformation, and

TABLE 1 Characteristic temperatures of the different transitions that take place in the polymer matrix, enthalpy of cold crystallization and melting, and degree of crystallinity of pure PLA and the different composite samples.

Sample	Glass transition (K)	Cold crystallization (K)	Melting (K)	Enthalpy (J g^{-1})		Degree of crystallinity (%)
				Cold crystallization	Melting	
Pure PLA	340.8	391.4	423	11.8	12.5	0.75
30 wt%	332.8	381.1	422.9–429.1	20.3	20.5	0.31
39 wt%	329.9	378.9	418.2–426.2	20.1	21.0	1.59
65 wt%	330.2	385.1	419.4–425.3	9.4	10.8	4.30

degree of crystallinity of pure PLA and the different composite samples. The degree of crystallinity, χ_c, that represents the percentage of crystalline polymer of the different filaments is estimated using the following equation:

$$\chi_c = \frac{\Delta H_m - \Delta H_{cc}}{w_p \cdot \Delta H_m^0} \cdot 100,$$

where ΔH_m is the enthalpy of melting, ΔH_{cc} the enthalpy related to the cold crystallization, w_p the weight fraction of polymer in the sample and $\Delta H_m^0 = 93\,\mathrm{J\,g^{-1}}$ the theoretical enthalpy of melting of 100% crystalline PLA.[56,62,63] The values obtained for the degree of crystallinity indicate that most of the polymer is in amorphous state in all the samples as the fused polymer that exits the nozzle of the extruder is quickly solidified. However, it is observed that the addition of the metallic fillers slightly increases the percentage of crystalline polymer with respect to that of pure PLA filament.

4 | MAGNETIC AND MAGNETOCALORIC CHARACTERIZATION

Considering that the magnetic moment in these PLA-based composites is exclusively due to the Ni-Mn-Ga fillers, an alternative quick and reliable way of determining the concentration is by comparing the mass magnetization of the raw powder and composite samples. Figure 7 shows the first quadrant of $M(H)$ at room temperature of the raw powder and composite filaments. For composites, magnetic particles are evenly distributed within a non-magnetic media with a maximum volume fraction of 0.227 (for the composite with 64 wt% of fillers), so that samples can have a larger demagnetizing factor compared with the compacted raw powder.[64] In fact, it was shown in a previous work that a polymer matrix with embedded spherical magnetic particles shows a demagnetizing factor close to that of a single particle (1/3) for low to medium vol% of fillers.[51] However, this

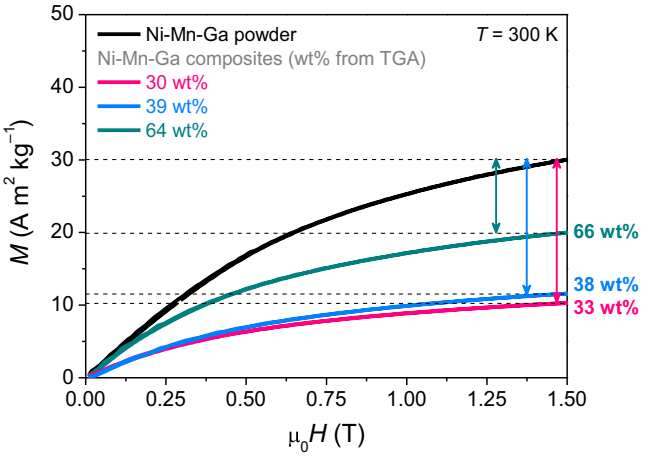

FIGURE 7 $M(H)$ magnetization curves of the off-stoichiometric Ni-Mn-Ga powder and composite filaments. The mass fraction of fillers in the composites is calculated by dividing their mass magnetization for 1.5 T by that of the raw powder.

would just affect the part of the $M(H)$ curves near the origin while the effect of the demagnetizing field is negligible close to saturation. Accordingly, the ratio between the mass magnetization of the composite samples for 1.5 T to that of the raw Ni-Mn-Ga powder directly gives the mass fraction of magnetic fillers within the composites, resulting in 33, 38, and 66 wt% of fillers in the composites with 30, 39, and 64 wt% of fillers according to the TGA characterization. In this way, not only the composition of the filaments is verified by alternative techniques but also it is confirmed that the functional property of the powder is retained after the filament fabrication.

Figure 8A shows the isothermal $M(H)$ curves measured upon increasing field using a discontinuous heating protocol for calculating ΔS_{iso}. It is observed a transition occurs from a ferromagnetic state at 250 K to a paramagnetic state at 400 K, which is associated to the Curie transition of the parent austenite as observed by the DSC characterization of the Ni-Mn-Ga powder of Figure 5. When the transformation upon heating takes place for fields below 0.5 T, a subtle magnetization increase is observed (i.e., the crossover of the $M(H)$ curves

highlighted with the gray arrow) indicating the occurrence of the martensitic transition in the Ni-Mn-Ga powder, for which the martensitic phase has a larger magnetic anisotropy than the high temperature austenitic one. This effect is common in these Heusler alloys.[65,66] This means that the magnetic response due to the FOPT is masked by the overlapping Curie transition of the austenite. The curves shown in Figure 8A have been used to numerically construct the heating isofield $M(T)$ curves presented in panel (B). The constructed $M(T)$ curves show more clearly the predominant ferro-to-paramagnetic Curie transition, revealing its gradual occurrence as well as the subtle magnetization increase in the 0.25 and 0.5 T curves, which can be attributed to the weaker magnetic response of the FOPT.

The $\Delta S_{iso}(T)$ curves for magnetic field changes up to 5 T of the raw powder are shown in Figure 9A. Despite the magnetostructural transformation in this type of Ni-Mn-Ga Heusler alloy would produce a sharp ΔS_{iso} peak, the observed response resembles more to that of a Curie transition, in accordance with the predominant behavior previously shown in panels of Figure 8. The exponent n, which defines the field dependence of ΔS_{iso} has been calculated to ascertain the occurrence of a magnetic FOPT by looking for a $n > 2$ overshoot.[67] Figure 9B shows the $n(T)$ curves for different magnetic fields calculated as:

$$n = \frac{dln|\Delta S_{iso}|}{dlnH}. \quad (4)$$

Values of n above 2 are clearly observed in the 3 T curve, which are followed by a minimum at ~350 K related to the Curie transition of the austenitic phase.

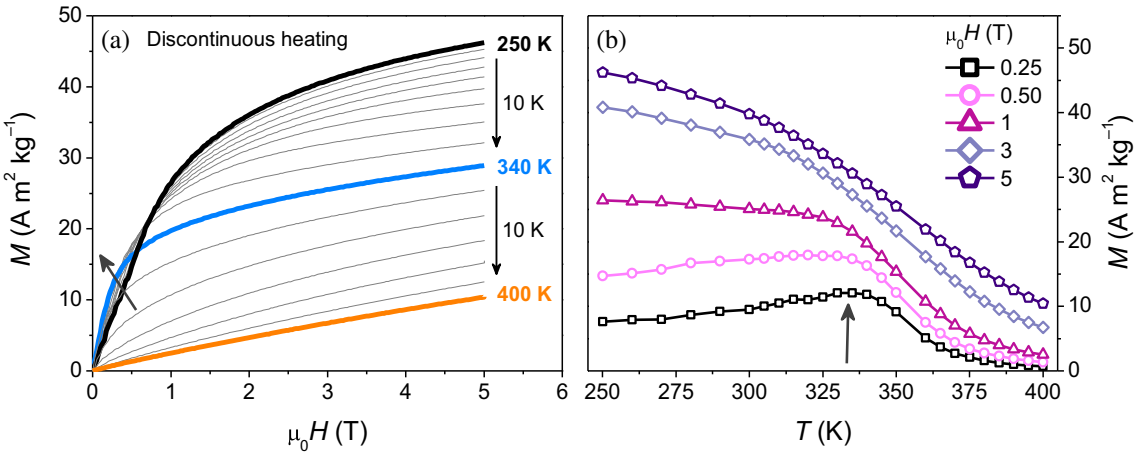

FIGURE 8 (A) $M(H)$ magnetization curves upon increasing field at different temperatures of the raw Ni-Mn-Ga. (B) Constructed $M(T)$ curves from the $M(H)$ data of (A).

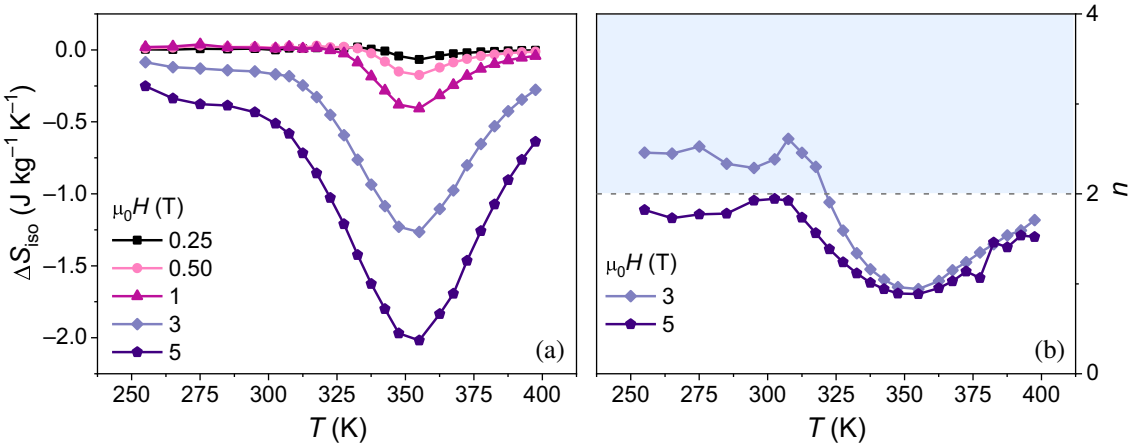

FIGURE 9 (A) Temperature dependence of ΔS_{iso} of the off-stoichiometric Ni_2MnGa powder for different magnetic field changes. (B) Temperature dependence of exponent n for fields changes of 3 and 5 T.

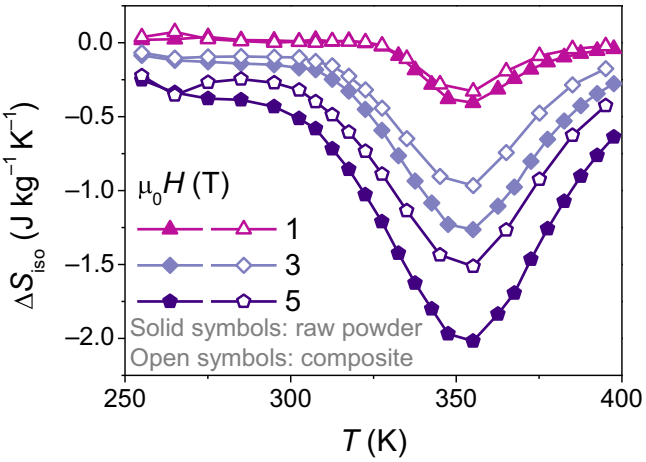

FIGURE 10 $\Delta S_{iso}(T)$ upon heating of the raw off-stoichiometric Heusler alloy powder (solid symbols) and composite of 64 wt% (open symbols).

This is an indication of an underlying magnetic FOPT, as previously determined by DSC, although its response seems to be masked by a predominant second-order one. In consequence, the overshoot of exponent n decreases with increasing magnetic field because the response of Curie transitions continuously increases in height and width with increasing field, while the FOPT response saturates from a certain field.

The MCE has also been characterized for the composite filament with the largest filling fraction (64 wt%) and it is presented in Figure 10 (open symbols) together with the response of the raw powder previously shown (solid symbols). The similarity of the curves of the two types of samples is evident, with a response in the composite, which is just scaled down due to the non-contributing mass of the polymer. As commented previously, the different demagnetizing factor that the two systems can have would not cause significant changes in the MCE curves above 1 T. The ratio of the peak responses of the raw powder and composite for 1 T is only slightly distorted with respect to the previously found ratio in the $M(H)$ at 1.5 T and the ratio between the MCE for 3 and 5 T.

5 | CONCLUSIONS

PLA-based composite filaments for FDM incorporating 30, 39, and 64 wt% of magnetocaloric off-stoichiometric Ni_2MnGa particles have been fabricated and characterized. For fabricating the filaments, the powder was filled and sealed into polymer capsules that were subsequently used as the feedstock for a single-screw extruder. It was found that the PLA with embedded particles had an increased flowability so the extrusion temperature for the composites had to be lowered. The morphology and particle distribution analysis from x-ray tomography experiments provide the volumetric fraction of fillers, indicating that particles are close together due to the high filling fraction achieved. This analysis also shows that particles are uniformly distributed, a characteristic that is essential for the manufacturing of parts with predictable functionality. The wt% of fillers has been determined from TGA measurements, with an estimated vol% from the densities of the components that is in good agreement with the result from x-ray tomography. Additionally, the TGA curves show that the degradation of PLA is displaced to lower temperatures with the addition of fillers. DSC measurements on the raw powder show the occurrence of a FOPT while those performed on the composites show changes in the thermal behavior of the polymer as the filling fraction increases. Among them, it is remarkable the effect of the fillers, acting as nucleation centers, promotes the cold crystallization with the appearance of higher fractions of the disordered crystalline phase of PLA. The magnetic and magnetocaloric characterization of raw powder and composites confirms that the method for fabricating the filaments preserves the functionality of the fillers, with a response that is proportional to the fraction of fillers. The procedure followed in this work allows to produce in one single extrusion step highly loaded composite filaments for FDM in which particles are uniformly distributed. The relatively low temperatures required for polymer extrusion are further reduced with increased filler content, which is beneficial for preserving the properties of the fillers as well as for saving energy and costs in manufacturing.

ACKNOWLEDGMENTS

Work funded by PID2019-105720RB-I00/AEI/10.13039/501100011033, Air Force Office of Scientific Research (FA8655-21-1-7044), and the Clean Hydrogen Partnership and its members within the project HyLICAL (grant no. 101101461). JYL acknowledges EMERGIA Fellowship from Junta de Andalucía (EMC21_00418). Atomization device was funded by POB "Technologie Materiałowe" of Warsaw University of Technology within the Excellence Initiative: Research University (IDUB) Programme.

CONFLICT OF INTEREST STATEMENT

The authors declare no conflicts of interest.

DATA AVAILABILITY STATEMENT

Data will be available upon reasonable request to the authors.

ORCID

Álvaro Díaz-García https://orcid.org/0000-0002-1400-5748

Jia Yan Law https://orcid.org/0000-0002-1431-6773

Victorino Franco https://orcid.org/0000-0003-3028-6815

REFERENCES

1. Franco V, Blázquez JS, Ipus JJ, Law JY, Moreno-Ramírez LM, Conde A. Magnetocaloric effect: from materials research to refrigeration devices. *Prog Mater Sci*. 2018;93:112-232. doi:10.1016/j.pmatsci.2017.10.005
2. Gutfleisch O, Willard MA, Brück E, Chen CH, Sankar SG, Liu JP. Magnetic materials and devices for the 21st century: stronger, lighter, and more energy efficient. *Adv Mater*. 2011;23(7):821-842. doi:10.1002/adma.201002180
3. Pecharsky VK, Gschneidner KA. Magnetocaloric effect and magnetic refrigeration. *J Magn Magn Mater*. 1999;200(1-3):44-56. doi:10.1016/S0304-8853(99)00397-2
4. Law JY, Moreno-Ramírez LM, Díaz-García Á, Franco V. Current perspective in magnetocaloric materials research. *J Appl Phys*. 2023;133(4):040903. doi:10.1063/5.0130035
5. Moreno-Ramírez LM, Law JY, Díaz-García Á, Franco V. Advanced magnetocaloric materials. *Encyclopedia of Materials: Electronics*. Elsevier; 2023:616-632. doi:10.1016/B978-0-12-819728-8.00068-1
6. Planes A, Mañosa L, Acet M. Magnetocaloric effect and its relation to shape-memory properties in ferromagnetic Heusler alloys. *J Phys Condens Matter*. 2009;21(23):233201. doi:10.1088/0953-8984/21/23/233201
7. Krenke T, Acet M, Wassermann EF, Moya X, Mañosa L, Planes A. Ferromagnetism in the austenitic and martensitic states of Ni-Mn-In alloys. *Phys Rev B*. 2006;73(17):1-10. doi:10.1103/PhysRevB.73.174413
8. Gottschall T, Skokov KP, Frincu B, Gutfleisch O. Large reversible magnetocaloric effect in Ni-Mn-In-Co. *Appl Phys Lett*. 2015;106(2):021901. doi:10.1063/1.4905371
9. Law JY, Díaz-García Á, Moreno-Ramírez LM, Franco V, Conde A, Giri AK. How concurrent thermomagnetic transitions can affect magnetocaloric effect: the Ni49+xMn36-xIn15 Heusler alloy case. *Acta Mater*. 2019;166:459-465. doi:10.1016/j.actamat.2019.01.007
10. Khan AN, Moreno-Ramírez LM, Díaz-García Á, Law JY, Franco V. All-d-metal Ni(Co)-Mn(X)-Ti (X = Fe or Cr) Heusler alloys: enhanced magnetocaloric effect for moderate magnetic fields. *J Alloys Compd*. 2023;931:167559. doi:10.1016/j.jallcom.2022.167559
11. Gutfleisch O, Gottschall T, Fries M, et al. Mastering hysteresis in magnetocaloric materials. *Philos Trans A Math Phys Eng Sci*. 2016;374(2074):20150308. doi:10.1098/rsta.2015.0308
12. Scheibel F, Gottschall T, Taubel A, et al. Hysteresis design of magnetocaloric materials-from basic mechanisms to applications. *Energ Technol*. 2018;6(8):1397-1428. doi:10.1002/ente.201800264
13. Díaz-García Á, Moreno-Ramírez LM, Law JY, Albertini F, Fabbrici S, Franco V. Characterization of thermal hysteresis in magnetocaloric NiMnIn Heusler alloys by temperature first order reversal curves (TFORC). *J Alloys Compd*. 2021;867:159184. doi:10.1016/j.jallcom.2021.159184
14. Ngo TD, Kashani A, Imbalzano G, Nguyen KTQ, Hui D. Additive manufacturing (3D printing): a review of materials, methods, applications and challenges. *Compos Part B Eng*. 2018;143(February):172-196. doi:10.1016/j.compositesb.2018.02.012
15. Prakash KS, Nancharaih T, Rao VVS. Additive manufacturing techniques in manufacturing—an overview. *Mater Today Proc*. 2018;5(2):3873-3882. doi:10.1016/j.matpr.2017.11.642
16. Mehrpouya M, Dehghanghadikolaei A, Fotovvati B, Vosooghnia A, Emamian SS, Gisario A. The potential of additive manufacturing in the smart factory industrial 4.0: a review. *Appl Sci*. 2019;9(18):3865. doi:10.3390/app9183865
17. Srivastava M, Rathee S, Patel V, Kumar A, Koppad PG. A review of various materials for additive manufacturing: recent trends and processing issues. *J Mater Res Technol*. 2022;21:2612-2641. doi:10.1016/j.jmrt.2022.10.015
18. Kamran MS, Sun J, Tang YB, Chen YG, Wu JH, Wang HS. Numerical investigation of room temperature magnetic refrigerator using microchannel regenerators. *Appl Therm Eng*. 2016;102:1126-1140. doi:10.1016/j.applthermaleng.2016.02.085
19. Lei T, Engelbrecht K, Nielsen KK, Veje CT. Study of geometries of active magnetic regenerators for room temperature magnetocaloric refrigeration. *Appl Therm Eng*. 2017;111:1232-1243. doi:10.1016/j.applthermaleng.2015.11.113
20. Frazier WE. Metal additive manufacturing: a review. *J Mater Eng Perform*. 2014;23(6):1917-1928. doi:10.1007/s11665-014-0958-z
21. Lewandowski JJ, Seifi M. Metal additive manufacturing: a review of mechanical properties. *Annu Rev Mat Res*. 2016;46(1):151-186. doi:10.1146/annurev-matsci-070115-032024
22. Toman J, Müllner P, Chmielus M. Properties of as-deposited and heat-treated Ni-Mn-Ga magnetic shape memory alloy processed by directed energy deposition. *J Alloys Compd*. 2018;752:455-463. doi:10.1016/j.jallcom.2018.04.059
23. Laitinen V, Sozinov A, Saren A, Salminen A, Ullakko K. Laser powder bed fusion of Ni-Mn-Ga magnetic shape memory alloy. *Addit Manuf*. 2019;30:100891. doi:10.1016/j.addma.2019.100891
24. Scheibel F, Lauhoff C, Riegg S, et al. On the impact of additive manufacturing processes on the microstructure and magnetic properties of Co–Ni–Ga shape memory Heusler alloys. *Adv Eng Mater*. 2022;24(10):2200069. doi:10.1002/adem.202200069
25. Miao X, Wang W, Liang H, et al. Printing (Mn,Fe)2(P,Si) magnetocaloric alloys for magnetic refrigeration applications. *J Mater Sci*. 2020;55(15):6660-6668. doi:10.1007/s10853-020-04488-8
26. Al-Milaji KN, Gupta S, Pecharsky VK, Barua R, Zhao H, Hadimani RL. Differential effect of magnetic alignment on additive manufacturing of magnetocaloric particles. *AIP Adv*. 2020;10(1):015052. doi:10.1063/1.5130028
27. Lejeune BT, Barua R, Simsek E, et al. Towards additive manufacturing of magnetocaloric working materials. *Materialia*. 2021;16:101071. doi:10.1016/j.mtla.2021.101071
28. Wang X, Jiang M, Zhou Z, Gou J, Hui D. 3D printing of polymer matrix composites: a review and prospective. *Compos Part B Eng*. 2017;110:442-458. doi:10.1016/j.compositesb.2016.11.034
29. Angelopoulos PM, Samouhos M, Taxiarchou M. Functional fillers in composite filaments for fused filament fabrication: a review. *Mater Today Proc*. 2021;37:4031-4043. doi:10.1016/j.matpr.2020.07.069
30. Yohannan A, Vincent S, Divakaran N, et al. Experimental and simulation studies of hybrid MWCNT/montmorillonite reinforced FDM based PLA filaments with multifunctional

properties enhancement. *Polym Compos*. 2023;45(1):507-522. doi:10.1002/pc.27794

31. Pinto GM, Cremonezzi JMO, Ribeiro H, Andrade RJE, Demarquette NR, Fechine GJM. From two-dimensional materials to polymer nanocomposites with emerging multifunctional applications: a critical review. *Polym Compos*. 2023;44(3):1438. doi:10.1002/pc.27213
32. Kumar J, Negi S. Development of 3D printable cenosphere-reinforced polyethylene terephthalate glycol (PETG) filaments for lightweight structural applications. *Polym Compos*. 2023;44(10):7030-7039. doi:10.1002/pc.27616
33. Tan JC, Low HY. Embedded electrical tracks in 3D printed objects by fused filament fabrication of highly conductive composites. *Addit Manuf*. 2018;23(June):294-302. doi:10.1016/j.addma.2018.06.009
34. Li R, Yang X, Li J, et al. Review on polymer composites with high thermal conductivity and low dielectric properties for electronic packaging. *Mater Today Phys*. 2022;22:100594. doi:10.1016/j.mtphys.2021.100594
35. Calascione TM, Fischer NA, Lee TJ, Thatcher HG, Nelson-Cheeseman BB. Controlling magnetic properties of 3D-printed magnetic elastomer structures via fused deposition modeling. *AIP Adv*. 2021;11(2):025223. doi:10.1063/9.0000220
36. Patton MV, Ryan P, Calascione T, et al. 3D printed magnetic polymer composite transformers. *Addit Manuf*. 2018;2018(27):97-101. doi:10.1016/j.addma.2018.06.009
37. Ganguly S, Margel S. 3D printed magnetic polymer composite hydrogels for hyperthermia and magnetic field driven structural manipulation. *Prog Polym Sci*. 2022;131:101574. doi:10.1016/j.progpolymsci.2022.101574
38. Aktitiz İ, Delibaş H, Topcu A, Aydın K. Morphological, mechanical, magnetic, and thermal properties of 3D printed functional polymeric structures modified with Fe_2O_3 nanoparticles. *Polym Compos*. 2021;42(12):6839-6846. doi:10.1002/pc.26344
39. Wan M, Jiang X, Nie J, et al. Phosphor powders-incorporated polylactic acid polymeric composite used as 3D printing filaments with green luminescence properties. *J Appl Polym Sci*. 2020;137(18):1-10. doi:10.1002/app.48644
40. Banerjee M, Jain A, Mukherjee GS. Microstructural and optical properties of polyvinyl alcohol/manganese chloride composite film. *Polym Compos*. 2019;40(S1):E765-E775. doi:10.1002/pc.25017
41. Frketic J, Dickens T, Ramakrishnan S. Automated manufacturing and processing of fiber-reinforced polymer (FRP) composites: an additive review of contemporary and modern techniques for advanced materials manufacturing. *Addit Manuf*. 2017;14:69-86. doi:10.1016/j.addma.2017.01.003
42. Hemath M, Mavinkere Rangappa S, Kushvaha V, Dhakal HN, Siengchin S. A comprehensive review on mechanical, electromagnetic radiation shielding, and thermal conductivity of fibers/inorganic fillers reinforced hybrid polymer composites. *Polym Compos*. 2020;41(10):3940-3965. doi:10.1002/pc.25703
43. Sharma V, Balderson L, Heo R, et al. Room-temperature polymer-assisted additive manufacturing of microchanneled magnetocaloric structures. *J Alloys Compd*. 2022;920:165891. doi:10.1016/j.jallcom.2022.165891
44. Díaz-García Á, Revuelta J, Moreno-Ramírez LM, Law JY, Mayer C, Franco V. Additive manufacturing of magnetocaloric $(La,Ce)(Fe,Mn,Si)_{13}$-H particles via polymer-based composite filaments. *Compos Commun*. 2022;35:101352. doi:10.1016/j.coco.2022.101352
45. Tosto C, Tirillò J, Sarasini F, Sergi C, Cicala G. Fused deposition modeling parameter optimization for cost-effective metal part printing. *Polymers*. 2022;14(16):3264. doi:10.3390/polym14163264
46. Lotfizarei Z, Mostafapour A, Barari A, Jalili A, Patterson AE. Overview of debinding methods for parts manufactured using powder material extrusion. *Addit Manuf*. 2023;61:103335. doi:10.1016/j.addma.2022.103335
47. Maga D, Hiebel M, Thonemann N. Life cycle assessment of recycling options for polylactic acid. *Resour Conserv Recycl*. 2019;149:86-96. doi:10.1016/j.resconrec.2019.05.018
48. Jagadeesh P, Mavinkere Rangappa S, Siengchin S, et al. Sustainable recycling technologies for thermoplastic polymers and their composites: a review of the state of the art. *Polym Compos*. 2022;43(9):5831-5862. doi:10.1002/pc.27000
49. Díaz-García Á, Law JY, Cota A, et al. Novel procedure for laboratory scale production of composite functional filaments for additive manufacturing. *Mater Today Commun*. 2020;24-(March):101049. doi:10.1016/j.mtcomm.2020.101049
50. Żrodowski Ł, Wróblewski R, Choma T, et al. Novel cold crucible ultrasonic atomization powder production method for 3D printing. *Materials*. 2021;14(10):2541. doi:10.3390/ma14102541
51. Díaz-García Á, Law JY, Felix M, Guerrero A, Franco V. Functional, thermal and rheological properties of polymer-based magnetic composite filaments for additive manufacturing. *Mater Des*. 2022;219:110806. doi:10.1016/j.matdes.2022.110806
52. Patton MV, Ryan P, Calascione T, et al. Manipulating magnetic anisotropy in fused filament fabricated parts via macroscopic shape, mesoscopic infill orientation, and infill percentage. *Addit Manuf*. 2019;27(March):482-488. doi:10.1016/j.addma.2019.03.026
53. Shenoy AV. *Rheology of Filled Polymer Systems*. 1st ed. Springer Netherlands; 1999. doi:10.1007/978-94-015-9213-0
54. Legland D, Arganda-Carreras I, Andrey P. MorphoLibJ: integrated library and plugins for mathematical morphology with ImageJ. *Bioinformatics*. 2016;32(22):btw413. doi:10.1093/bioinformatics/btw413
55. Tocado L, Palacios E, Burriel R. Entropy determinations and magnetocaloric parameters in systems with first-order transitions: study of MnAs. *J Appl Phys*. 2009;105(9):093918. doi:10.1063/1.3093880
56. Caron L, Ou ZQ, Nguyen TT, Cam Thanh DT, Tegus O, Brück E. On the determination of the magnetic entropy change in materials with first-order transitions. *J Magn Magn Mater*. 2009;321(21):3559-3566. doi:10.1016/j.jmmm.2009.06.086
57. Kaeswurm B, Franco V, Skokov KP, Gutfleisch O. Assessment of the magnetocaloric effect in La,Pr(Fe,Si) under cycling. *J Magn Magn Mater*. 2016;406:259-265. doi:10.1016/j.jmmm.2016.01.045
58. Karakoç A, Rastogi VK, Isoaho T, Tardy B, Paltakari J, Rojas OJ. Comparative screening of the structural and thermomechanical properties of FDM filaments comprising thermoplastics loaded with cellulose, carbon and glass fibers. *Materials*. 2020;13(2):422. doi:10.3390/ma13020422
59. Sang L, Han S, Peng X, Jian X, Wang J. Development of 3D-printed basalt fiber reinforced thermoplastic honeycombs with enhanced compressive mechanical properties. *Compos Part A Appl Sci Manuf*. 2019;125(July):105518. doi:10.1016/j.compositesa.2019.105518

60. Durmus A, Ercan N, Soyubol G, Deligöz H, Kaşgöz A. Nonisothermal crystallization kinetics of poly(ethylene terephthalate)/clay nanocomposites prepared by melt processing. *Polym Compos*. 2010;31(6):1056-1066. doi:10.1002/pc.20892
61. Coppola B, Cappetti N, Di ML, Scarfato P, Incarnato L. 3D printing of PLA/clay nanocomposites: influence of printing temperature on printed samples properties. *Materials*. 2018; 11(10):1-17. doi:10.3390/ma11101947
62. Kong Y, Hay JN. The measurement of the crystallinity of polymers by DSC. *Polymer*. 2002;43(14):3873-3878. doi:10.1016/S0032-3861(02)00235-5
63. Zhang C, Lan Q, Zhai T, Nie S, Luo J, Yan W. Melt crystallization behavior and crystalline morphology of polylactide/poly(ε-caprolactone) blends compatibilized by lactide-caprolactone copolymer. *Polymers*. 2018;10(11):1181. doi:10.3390/polym10111181
64. Coey JMD. *Magnetism and Magnetic Materials*. Cambridge University Press; 2001. doi:10.1017/CBO9780511845000
65. Duan J, Huang P, Zhang H, et al. Negative and positive magnetocaloric effect in Ni–Fe–Mn–Ga alloy. *J Magn Magn Mater*. 2007;309(1):96-99. doi:10.1016/j.jmmm.2006.06.017
66. Kikuchi D, Kanomata T, Yamaguchi Y, Nishihara H, Koyama K, Watanabe K. Magnetic properties of ferromagnetic shape memory alloys Ni2Mn1−Fe Ga. *J Alloys Compd*. 2004;383(1–2):184-188. doi:10.1016/j.jallcom.2004.04.053
67. Law JY, Franco V, Moreno-Ramírez LM, et al. A quantitative criterion for determining the order of magnetic phase transitions using the magnetocaloric effect. *Nat Commun*. 2018;9(1): 2680. doi:10.1038/s41467-018-05111-w

How to cite this article: Díaz-García Á, Law JY, Żrodowski Ł, Morończyk B, Wróblewski R, Franco V. Polymer-based filaments with embedded magnetocaloric Ni-Mn-Ga Heusler alloy particles for additive manufacturing. *Polym Compos*. 2024; 1-13. doi:10.1002/pc.28130